Presented at the Topical Meeting on Free Electron
Generation of Extreme UV Coherent Radiation.
Brookhaven National Laboratory, 9/19-22/83.

BNL-34340

BNL--34340

CONF-830911/8--8

DE84 006172

Collective Instabilities and High-Gain Regime Free Electron Laser

R. Bonifacio*, C. Pellegrini
National Synchrotron Light Source
Brookhaven National Laboratory
Upton, NY 11973

and

L.M. Narducci
Department of Physics & Atmospheric Science
Drexel University
Philadelphia, PA 19104

*On leave from the University of Milano, Via Celoria 16,
Milano, Italy

1. INTRODUCTION

The operation of Free Electron Lasers (FEL) in the short wavelength region, $\lambda < 1000$ Å, requires a large field amplification per undulator pass in order to overcome the large losses of the optical cavity at these wavelengths[1]. Systems based on the combination of a storage ring and of a free electron laser can provide this large amplification[2,3]. In fact, for these systems small-signal gains of the order of 100-1000% per pass have been estimated. Of course, at this level of amplification, the small-signal gain formula is no longer appropriate and a more accurate description of the FEL is required.

FEL studies in the high-gain regime have been carried out by many authors[4-11] who have shown that, with an appropriate selection of the electron density, detuning, and undulator length, it is possible to produce an exponential growth of both the radiation field and of the electron bunching. This is the result of the emergence of a collective instability for the electron beam-undulator-radiation field system.

In this paper we study the conditions for the onset of this instability and derive the characteristic complex frequencies of the FEL system which are different from the ones derived in Refs. 4 and 11. We show from this result how one can obtain the small-signal gain formula and establish the condition for its validity. We also consider the problem of the initiation of laser action and of the growth of the radiation field from noise and derive a formula to evaluate the lethargy time. Finally, we study numerically the nonlinear regime and obtain results related to the maximum amplification and optimum efficiency of the FEL.

No space-charge effects are included in our description so that we limit our considerations to cases where the ratio of the plasma frequency to undulator frequency is sufficiently smaller than unity.

2. THE FEL EQUATIONS

Following earlier developments[12,13] we derive the working equations of the FEL using the phase and energy as electron variables and the slowly varying phase and amplitude approximation for the radiation field. In this and the remaining sections, we shall adopt the following notations: z represents the direction of propagation of the electron beam and of the electromagnetic wave, as well as the undulator axis; x and y are the transverse coordinates; B_o denotes the undulator magnetic field (we use a helical undulator for simplicity) and λ_o and N_o the period length and the number of periods, repsectively; the undulator parameter is $\kappa = eB_o\lambda_o/(2\pi mc^2)$, where mc^2 is the electron rest energy; λ is the wavelength of the radiation field, γ is the electron energy in units of mc^2, β_z is the longitudinal electron velocity and $\beta_p = \kappa/\gamma$ the amplitude of the transverse velocity; the electron phase, ϕ, relative to that of the electromagnetic wave is connected to z and t by the relation $\phi = 2\pi z/\lambda_o + 2\pi(z-ct)/\lambda$; the resonant energy γ_R is related to λ_o, λ and κ by $\gamma_R^2 = \lambda_o(1+\kappa^2)/2\lambda$, and, finally, the undulator frequency ω_o is given by $\omega_o = 2\pi c\beta_z/\lambda_o$.

With these notations, the FEL equations can be written as[12,13]:

$$\dot{\phi}_j = \omega_o(1 - \gamma_R^2/\gamma_j^2) \qquad (1)$$

$$\dot{\gamma}_j = -\frac{ec\kappa}{2mc^2\gamma_j}\left(\alpha\, e^{i\phi_j} + c.c.\right) \tag{2}$$

$$\left(\frac{\partial}{\partial z} + \frac{1}{c}\frac{\partial}{\partial t}\right)\alpha = 2\pi\, n_e (z - \langle\beta_z\rangle ct)\,\frac{\kappa}{\Sigma}\left\langle \frac{e^{-i\phi}}{\gamma}\right\rangle_{(z = \langle\beta_z\rangle ct)} \tag{3}$$

where j labels the j-th electron in the beam ($j=1,2,\ldots,N_e$, with N_e being the total number of electrons), the average $\langle\ldots\rangle$ is carried out over all electrons in a beam slice of length λ at the beam position $z - \langle\beta_z\rangle ct$ where $\langle\beta_z\rangle$ is the average longitudinal velocity. The remaining parameters have the following meanings: n_e is the electron beam longitudinal density, Σ is an effective beam transverse cross section describing the overlap of the beam with the radiation field, whose amplitude E_o and phase θ_o have been combined in the complex amplitude

$$\alpha = i\, E_o\, e^{i\theta_o} \tag{4}$$

It is important to stress that, contrary to what was done in Refs. 12,13, we have not required that γ remain nearly the same as the resonant value γ_R throughout the evolution.

For the purpose of our subsequent analysis, it is convenient to rewrite Eqs. (1),(2) and (3) using the variables

$$\begin{cases} z' = z - \langle\beta_z\rangle ct \\ t' = t \end{cases} \tag{5}$$

In this case, these equations become

$$\frac{\partial}{\partial t'}\,\phi_j = \omega_o\left(1 - \gamma_R^2/\gamma^2\right) \tag{6}$$

$$\frac{\partial}{\partial t'}\,\gamma_j = -\frac{ec\kappa}{2mc^2\gamma_j}\left(\alpha\, e^{i\phi_j} + c.c.\right) \tag{7}$$

$$\left[(1 - \beta_z)\frac{\partial}{\partial z'} + \frac{1}{c}\frac{\partial}{\partial t'}\right] a = 2\pi\, n_e(z')\,\frac{K}{\Sigma}\left\langle \frac{e^{-i\phi}}{\gamma}\right\rangle_{z'} \tag{8}$$

The term $(1 - \beta_z)\partial/\partial z'$ in Eq. (8) is important to describe the pulse propagation in a FEL, especially when the electron-photon slippage $N_o\lambda$ in crossing the undulator is comparable to the length of the electron bunch, L_e. In this paper we confine ourselves to the situation where $L_e >> N_o\lambda$; thus, we neglect the propagation term $(1 - \beta_z)\partial/\partial z'$ and assume that the electron density $n_e(z')$ is constant and equal to n_o.

3. STABILITY ANALYSIS

The FEL equations (6)-(8) are more conveniently analyzed in terms of a new set of variables and parameters. We will use the relativistic beam plasma frequency

$$\Omega_p = \left[\frac{4\pi r_e n_o c^2}{\gamma_o^2}\right]^{1/2} \tag{9}$$

where γ_o is the initial enectron energy and r_e the classical radius of the electron; we also introduce the quantities

$$\rho = \left[\frac{K}{4}\,\frac{\gamma_o^2}{\gamma_R}\,\frac{\Omega_p}{\omega_o}\right]^{2/3} \tag{10}$$

and

$$\dot{\phi}_o = \omega_o(1 - \gamma_R^2/\gamma_o^2) \tag{11}$$

and rescale the time variable as

$$\tau = 2\omega_o\,\rho(\gamma_R/\gamma_o)^2\,t \tag{12}$$

In terms of the new variables:

$$\psi = \phi - \dot{\phi}_o t \tag{13}$$

$$\Gamma = \frac{1}{\rho}\frac{\gamma}{\gamma_o} \tag{14}$$

$$A = \frac{\alpha\, e^{i\dot{\phi}_o t}}{(4\pi\, mc^2 \gamma_o n_o \rho^2)^{1/2}} \tag{15}$$

Eqs. (6)-(8) become

$$\psi_j' = \frac{1}{2\rho}\left(1 - 1/\rho^2\Gamma_j^2\right) \tag{16}$$

$$\Gamma_j' = -\frac{1}{\rho}\left[\frac{A}{\Gamma_j}\, e^{i\psi_j} + c.c.\right] \tag{17}$$

$$A' = i\delta A + \frac{1}{\rho}\left\langle \frac{e^{-i\psi}}{\Gamma} \right\rangle \tag{18}$$

where the prime denotes differentiation with respect to the new scaled time variable. Equations (16)-(18) represent our working description for the dynamics of the FEL; they are controlled by the two parameters ρ, the Pierce parameter, and

$$\delta = \Delta/\rho \tag{19}$$

where Δ is the usual detuning parameter

$$\Delta = \frac{\gamma_o^2 - \gamma_R^2}{2\gamma_R^2} \tag{20}$$

Because we neglect space-charge forces, we assume in the following that ρ is sufficiently smaller than unity. Using the above equations of motion, one can easily verify that the quantity

$$L = \langle\Gamma\rangle + |A|^2 \tag{21}$$

is an invariant. In terms of measurable parameters, Eq. (21) can also be written as:

$$L = mc^2 n_o \langle\gamma\rangle + E_o^2/4\pi = \text{const} \tag{22}$$

which can easily be recognized as the conservation of energy for the electron beam-radiation field system.

In our subsequent numerical studies of the equations of motion (16)-(18), the maximum time is defined by the undulator length, $t_{max} = N_o\lambda_o/c$. In terms of the scaled time τ this becomes

$$\tau_{max} = 4\pi\rho\left(\frac{\gamma_o}{\gamma_R}\right)^2 N_o \tag{23}$$

which, for typical parameters $\rho = 10^{-2}$, $\gamma_o \approx \gamma_R$ and $N_o = 10^2$ leads to $\tau_{max} \sim 4\pi$.

We have analyzed the stability of this system following the method developed by Bonifacio, Casagrande and Casati[11]. The equations are linearized around the equilibrium state $A_o=0$, $\Gamma_{oj} = 1/\rho$, $\langle e^{-in\psi_o}\rangle = 0$, and perturbed by letting $A=a$, $\Gamma_j = \frac{1}{\rho}(1+\eta_j)$, $\psi_j = \psi_{oj} + \psi_j$. The linearized equations for the variables a,η, and ψ can be used to construct linear equations for the collective variables

$$x = \langle\psi\, e^{-i\psi_o}\rangle \tag{24}$$

$$y = \frac{1}{\rho}\langle\eta\, e^{-i\psi_o}\rangle \tag{25}$$

These take the form

$$X' = Y \tag{26}$$

$$Y' = -a \tag{27}$$

$$a' = i\delta a - iX - \rho Y \tag{28}$$

Nontrivial solutions with a time dependence of the type $e^{i\lambda\tau}$ will exist if λ is a solution of the characteristic equation:

$$\lambda^3 - \delta\lambda^2 + \rho\lambda + 1 = 0 \qquad (29)$$

This differs from the secular equation derived in previous publications[4,11] because of the linear term $\rho\lambda$ whose origin can be traced to our retention of the variable Γ inside the average carried out in the last term of Eq. (18). The results of the earlier analyses[4,11] can be obtained by formally setting $\rho = 0$ in Eq. (29). The solutions of the linearized equations (26)-(28) will exhibit exponential growth corresponding to the emergence of an instability if the cubic equation (29) has one real and two complex conjugate roots. In this case, the imaginary part of the eigenvalue measures the rate of growth of the unstable solution. The instability condition can be derived easily[14]: in terms of the parameters ρ and δ it takes the form

$$\rho^3 - \frac{1}{4}\rho^2\delta^2 + \frac{9}{2}\rho\delta - \delta^3 + \frac{27}{4} > 0 \qquad (30)$$

The boundary between the stable and unstable domains of equations (26)-(28) is shown in Fig. 1. Obviously, ρ is a positive definite quantity, so that for any value of δ less than δ^* (see Fig. 1) the equations of motion will always lead to unstable behavior. Only for $\delta > \delta^*$ will one need to overcome a threshold condition in order to produce an exponential growth of the initial signal.

The eigenvalues of the linearized system, not surprisingly, are responsible for many key aspects of the problem; they control the emergence of instabilities, the duration of the build-up time of the pulse, and the system's small signal gain.

Figure 2 shows the dependence of a typical set of eigenvalues on the detuning parameter δ. As expected from the shape of the instability boundary (Fig. 1), the eigenvalues are real beyond a given value δ_{thr}

of the detuning parameter, while two of them are complex conjugate of each other for $\delta<\delta_{thr}$. Of course, the threshold value depends on ρ.

For $\rho \ll 1$, the imaginary part of the eigenvalues display a characteristic power law dependence on δ near the instability threshold and for large values of the detuning parameter. Thus, a simple analysis shows that

$$\text{Im}\,\lambda \sim |\delta|^{-1/2}, \quad |\delta| \gg 1 \tag{31a}$$

$$\text{Im}\,\lambda \sim (\delta_{thr}-\delta)^{1/2}, \quad \delta \approx \delta_{thr} \tag{31b}$$

In particular, Eq. (31b) may be recognized as the typical behavior of the rate constant in the neighborhood of an instability threshold.

4. THE SMALL-SIGNAL GAIN

The small-signal gain emerges in a natural way from our analysis in the limit $\rho \to 0$ and for sufficiently large values of $|\delta|$. In this case, the eigenvalues take the explicit limiting form (to order $1/\delta$)

$$\lambda_1 \simeq \delta\left(1 - \frac{1}{\rho}\right), \lambda_{2,3} \simeq \pm \frac{1}{\delta^{1/2}}, \quad \delta > 0 \tag{32a}$$

$$\lambda_1 \simeq \delta\left(1 - \frac{1}{\rho}\right), \lambda_{2,3} \simeq \pm \frac{1}{|\delta|^{1/2}}, \quad \delta < 0 \tag{32b}$$

as one can confirm qualitatively by inspection of Fig. 2. It is now a simple matter to calculate the output field in the linear regime where $A(\tau)$ is just a linear combination of exponentials

$$A(\tau) = \sum_{j=1}^{3} C_j e^{i\lambda_j \tau} \tag{33}$$

and where C_j are constants to be determined from the initial conditions. A lengthy, but straightforward calculation yields the following expressions for the small-signal gain:

$$G \equiv \frac{|A(\tau)|^2 - |A_o|^2}{|A_o|^2} = \frac{4}{\delta^3}\left(1 - \cos\delta\tau\cos\frac{\tau}{\sqrt{\delta}} + \frac{1}{2}\delta^{3/2}\sin\delta\tau\sin\frac{\tau}{\sqrt{\delta}}\right), \quad \delta > 0 \tag{34a}$$

$$G = \frac{4}{\delta^3}\left(1 - \cos\delta\tau\cosh\frac{\tau}{\sqrt{|\delta|}} + \frac{1}{2}|\delta|^{3/2}\sin\delta\tau\sin\frac{\tau}{\sqrt{|\delta|}}\right), \quad \delta < 0 \tag{34b}$$

To make contact with what is usually known as the small-signal gain formula[12,13] it is not enough to require that $|\delta|$ be sufficiently larger than unity, but one alsom must impose the condition $\frac{\tau}{\sqrt{|\delta|}} \ll 1$. In this case, Eqs. (34) take the form

$$G \simeq \frac{4}{\delta^3}\left(1 - \cos\delta\tau + \frac{\delta\tau}{2}\sin\delta\tau\right) \tag{35}$$

which, in fact, agrees with the standard expression for G.

5. TIME EVOLUTION OF THE FREE ELECTRON LASER

The analysis of the time evolution of the system as prescribed by the nonlinear equations (16)-(18) requires, in general, a numerical approach. Two aspects of this problem can still be handled very accurately by analytical means.

(i) Evolution Below Threshold

When the detuning parameter is sufficiently large that the system operates stably below threshold, the time evolution of the output intensity is very well described by the linear approximation (33). In this regime, the eigenvalues are real and the output field displays small amplitude oscillations when plotted as a function of time. On varying δ, the real eigenvalues undergo significant variations, as one can see from Fig. 2, so that, depending on the values of the operating parameters, a variety of different output patterns can be obtained. These include beats, as well as more complicated modulation phenomena. The origin of these oscillations, however, can be understood entirely with reference to the eigenvalues of the linearized problem. Two examples are shown in Figs. 3 and 4, which are representative of the patterns that characterize the operation below threshold. It may be worth mentioning that while the traces shown in Figs. 3 and 4 have been produced by plotting Eq. (33), the exact solution of the nonlinear equations (16)-(18) is indistinguishable on the scale of these graphs.

(ii) Short-time Evolution and Lethargy

If the initial bunching parameter $|\langle e^{-i\psi_o}\rangle|$ were exactly equal to zero and all the electrons were injected in the active region with the same velocity, and if in addition, the initial field amplitude is zero, the field source term would be exactly zero and no emission would occur. In fact, the mechanisms that trigger the initial field build-up are the presence of fluctuations in the electron injection velocities, or the lack of uniformity in the initial distribution of the electron phase variables, or the presence of an initial field. In this paper we have

studied the evolution triggered by an initial small value of the bunching parameter, but the same conclusion would apply if one injected a small initial field and set the initial bunching parameter equal to zero. Because of the nature of the triggering mechanism, intuitively, one would expect that the time required for the initial pulse to build up (lethargy time) should be a rather sensitive function of the initial bunching parameter. We have examined the dependence of the first pulse build-up time on the initial value of the bunching parameter and verified that:

(1) a significant fraction of the build-up process is well described by the solution of the linearized equations; and

(2) the arrival time of the first peak is described to an excellent approximation by the formula:

$$\tau_{peak} = -\frac{1}{2Im\lambda} \ln |\langle e^{-i\psi_o} \rangle| + 1 \qquad (36)$$

Thus, one can expect significant fluctuations in the lethargy time. On the other hand, we have also verified that the peak height $|A_{max}|^2$ is essentially independent of the number of electrons n_o, as long as n_o is larger than about 30. In these simulations, we have assumed that all the electrons are injected with the same velocity.

A test of point (1) above is given in Fig. 5 where numerical solutions of Eqs. (16)-(18) are compared with those solutions of the linearized equations (33). As one can see, most of the build-up time is well represented by the linearized exponential growth. A comparison of Eq. (36) with the calculated values of τ_{peak} from Eqs. (16)-(18) is shown in Fig. 6.

We have analyzed the full nonlinear regime using the exact equations of motion under the assumption that all the injected electrons have the same initial velocity. One aspect of considerable interest for the purpose of optimizing the system's parameters is the existence of a maximum peak power output as a function of ρ and δ. We can see that while a maximum initial growth rate is obtained for $\delta \simeq 0$, the maximum peak amplitude occurs for $\delta \simeq \delta_{thr}$. We have analyzed this point by monitoring the peak output intensity of the FEL just above threshold (i.e., by selecting the parameters ρ and δ as close as practical to the boundary curve of Fig. 2). The results of this scan are displayed in Fig. 7 where the peak output intensity $\rho|A|^2_{max}$ is plotted as a function of ρ. The scatter of the points is almost certainly due to the slight variation of the conditions from run to run. The solid line which is only a qualitative average through the points, suggests the existence of an optimum gain condition such that the efficiency of the system is maximum for operation just above threshold. We find remarkable that at least in principle, efficiencies as high as about 40% should be available. It is also clear that treatments in which the initial electron momentum is assumed to vary only by a small amount during the evolution cannot be adequate to describe situations where such large energy exchanges take place between the electron beam and the field.

The above results are somewhat sensitive to the initial momentum spread of the electron beam. In Fig. 8 we show some preliminary results of a comparison between output pulses generated with different initial amounts of momentum spread. The general trend is a lowering of the maximum pulse intensity and a reduction of the lethargy time. This point, however, will require additional investigation.

We conclude with a brief comment concerning the connection between the results predicted on the basis of the present equations (16)-(18) and of those proposed in Ref. 11. We note that the main difference between our present treatment and that of Bonifacio, Casagrande and Casati is that, in the present treatment, the electron momenta are allowed to vary appreciably with respect to their initial values. It is expected, then, that for sufficiently low values of the Pierce parameter, when the electron energy suffers only a limited depletion, the two sets of equations should yield essentially identical results. A verification of this statement is given in Fig. 9.

ACKNOWLEDGEMENTS

One of us (LMN) wishes to acknowledge the support of the Army Research Office and the Research Laboratories of the Martin-Marietta Corporation. The help of D.K. Bandy and H. Sadiky with some of the numerical computations is also gratefully acknowledged. This work has been partially supported by the U.S. Department of Energy.

REFERENCES

1. See, for example, the report of the working group on optics in this proceedings volume.

2. C. Pellegrini, Nuclear Instruments and Methods, 177, 227 (1980).

3. J.M.J. Madey, in this proceedings volume.

4. N.M. Kroll and W.A. McMullin, Phys. Rev. A17, 300 (1978).

5. A. Gover and Z. Livni, Opt. Comm. 26, 375 (1978).

6. I.B. Bernstein and J.L. Hirshfeld, Phys. Rev. A20, 1661 (1979).

7. C.C. Shil and A. Yariv, IEEE J. Of Quantum Electron., QE-17, 1387 (1981).

8. P. Sprangle, C.M. Tang and W.M. Manheimer, Phys. Rev. A20, 302, (1980).

9. G. Dattoli, A. Marino, A. Renieri, F. Romanelli, IEEE J. of Quantum Electron., QE-17, 1371 (1981).

10. A. Gover, P. Sprangle, IEEE J. of Quantum Electron., QE-17, 1196 (1981).

11. R. Bonifacio, F. Casagrande and G. Casati, Opt. Comm. 40, 219 (1982).

12. W.B. Colson and S.K. Ride, in "Physics of Quantum Electronics", edited by S.F. Jacobs et al., (Addison-Wesley, Reading, MA 1980), Vol. 7, p.377.

13. C. Pellegrini in "Physics and Technology of Free Electron Lasers", Erice Italy (1980), edited by A.N. Chester et al. (to be published).

14. M. Abramowitz and I.A. Stegun, "Handbook of Mathematical Functions", Dover Publications, NY, 1970, eq. 3.8.2, p. 17.

FIGURE CAPTIONS

(1) Instability boundary in the (ρ,δ) plane. For $\delta<\delta^*$ the solutions of Eqs. (16)-(18) are unstable for all values of ρ which is a positive definite quantity. For a selected value of ρ (e.g. $\bar{\rho}$ in the figure) unstable behavior occurs for $\delta<\delta_{thr}$.

(2) The behavior of three eigenvalues of the secular equation as a function of the detuning parameter δ and for $\rho = 0.1$. The vertical axis labels both the real and imaginary parts. The real parts have been scaled by a factor of 10 to fit the display. For a sufficiently postive value of δ (i.e., $\delta > \delta_{thr}$). The eigenvalues are real (curves c,d,e). At threshold, two the real eigenvalues degenerate into one, while, for the same value of δ, the imaginary parts (curves b,b') become different from zero. The real part of the complex conjugate eigenvalues for $\delta < \delta_{thr}$ is labelled by a.

(3) Output intensity $|A|^2$ as a function of time for $\rho = 0.01$ and $\delta = 10$. The eigenvalues of the linearized problem are -0.347, 0.364, 7.90. The beat pattern is due to the interference between the first two eigenvalues, while the rapid oscillations are produced by the third. The horizontal time axis ranges from 0 to 20 units of τ. The vertical axis has been expanded from 9.0×10^{-4} to 1.15×10^{-4} to display the oscillations.

(4) Output intensity $|A|^2$ for $\rho = 0.01$ and $\delta = 4.0$. The eigenvalues of the linearized equations are -0.519, 0.628, 3.066. The beat pattern is no longer observable over the scale (0,40) fo the time axis. The vertical axis ranges from 0.0 to 2.0×10^{-4}.

(5) Comparison between the exact solution of the FEL equations and the exponential growth predicted by the linearized approximations.

(6) The arrival time of the first peak (lethargy time) is plotted as a function of the logarithm of the initial bunching parameter (dots). The solid curve corresponds to Eq. (36). The parameters used in this scan are $n_o = 8$, $\rho = 0.4$, $\delta = 1.25$.

(7) Dependence of the peak output intensity $|A|^2_{max}$ on ρ in the neighborhood and just above the instability boundary line of Fig. 1. The solid line is only a qualitative average of the points.

(8) The effect of an initial momentum spread. The output pulses have been obtained for $n_o = 16$, $\rho = 0.01$ and $\delta = 1.0$ and are displayed on a time scale from 0-12 units of τ. From right to left the initial spread, $\delta\gamma/\gamma$, equals 0, 5×10^{-4} 5×10^{-3}

(9) A comparison between the solution of our equations (16)-(18) and those of Ref. 11. The parameters used in this simulation are $\rho = 0.0021$, $\delta = 1.86$, $n_o = 16$. The horizontal axis ranges from 0-20 units of τ.

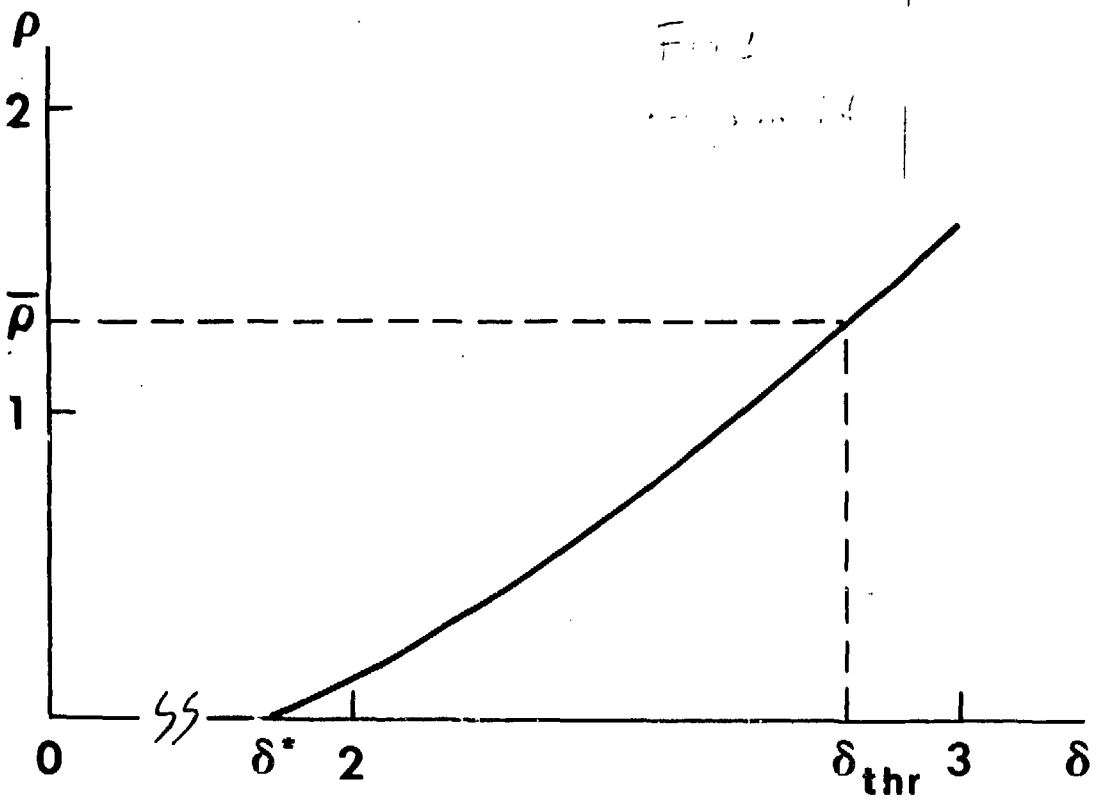
ρ
2
ρ̄
1
0
δ*
2
δthr
3
δ

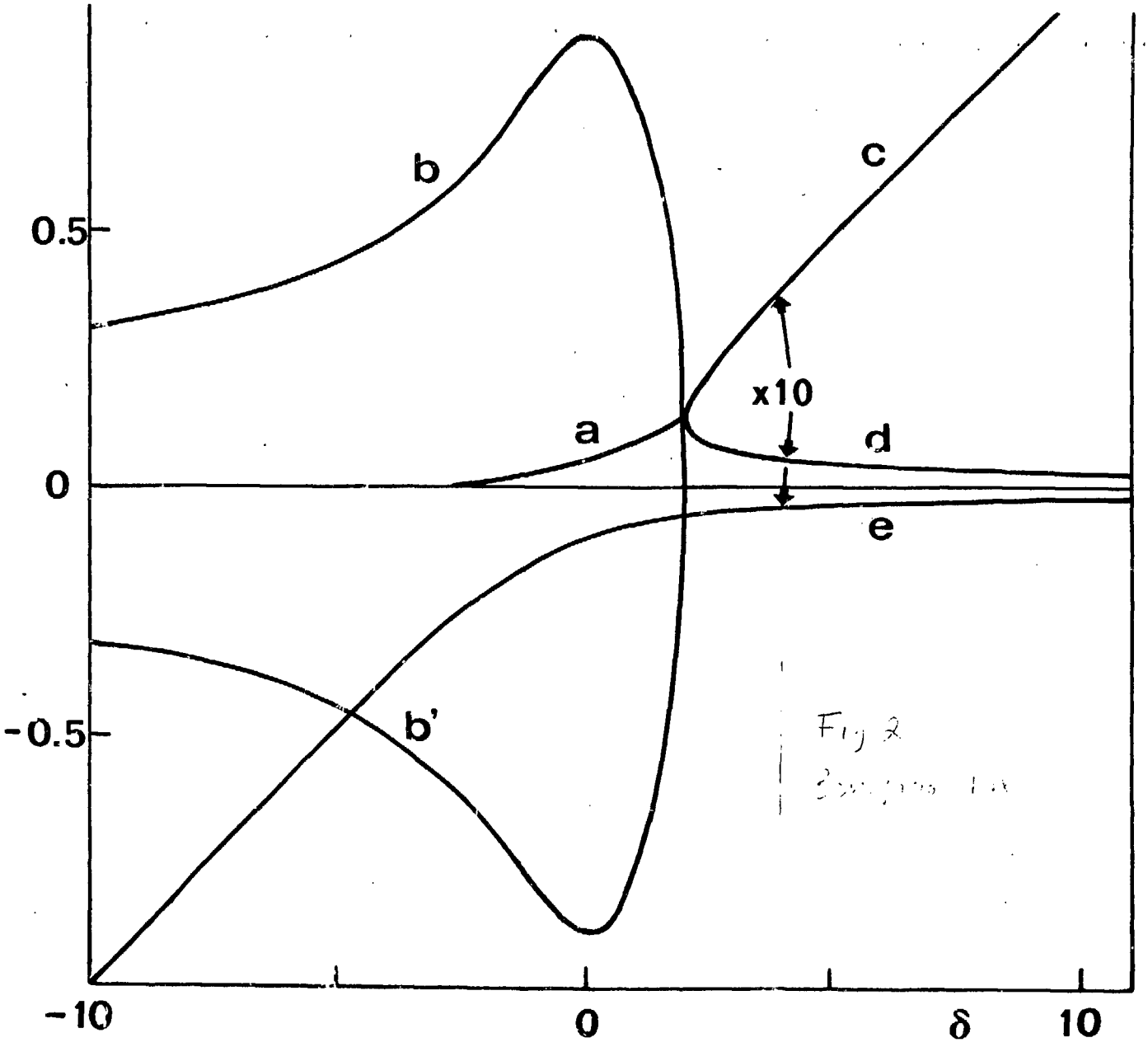

Fig 2

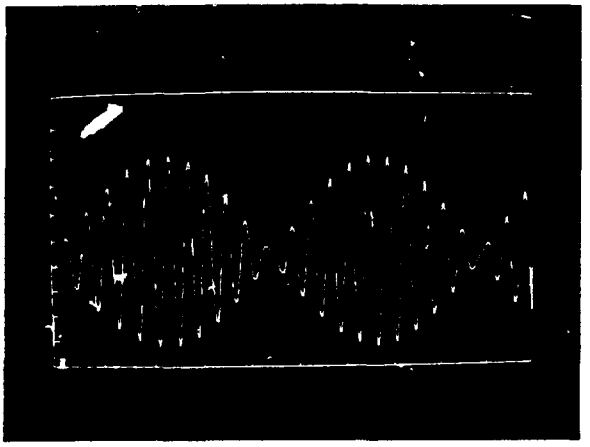

Fig 3

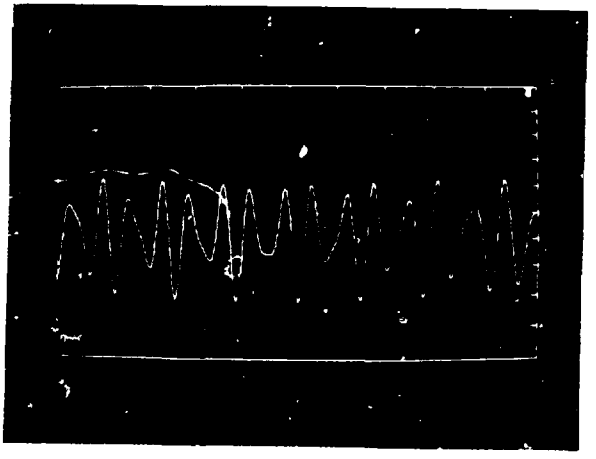

Fig 4

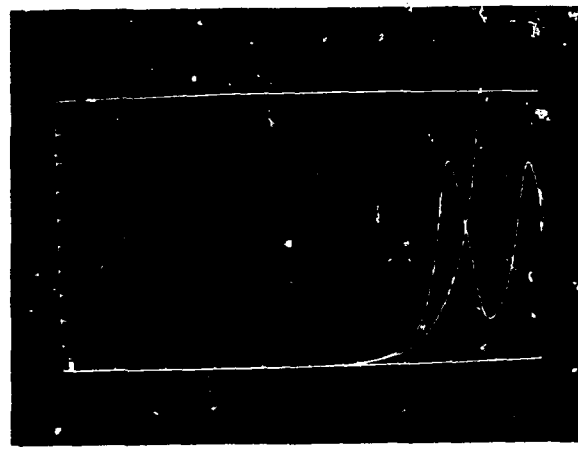

Fig 5

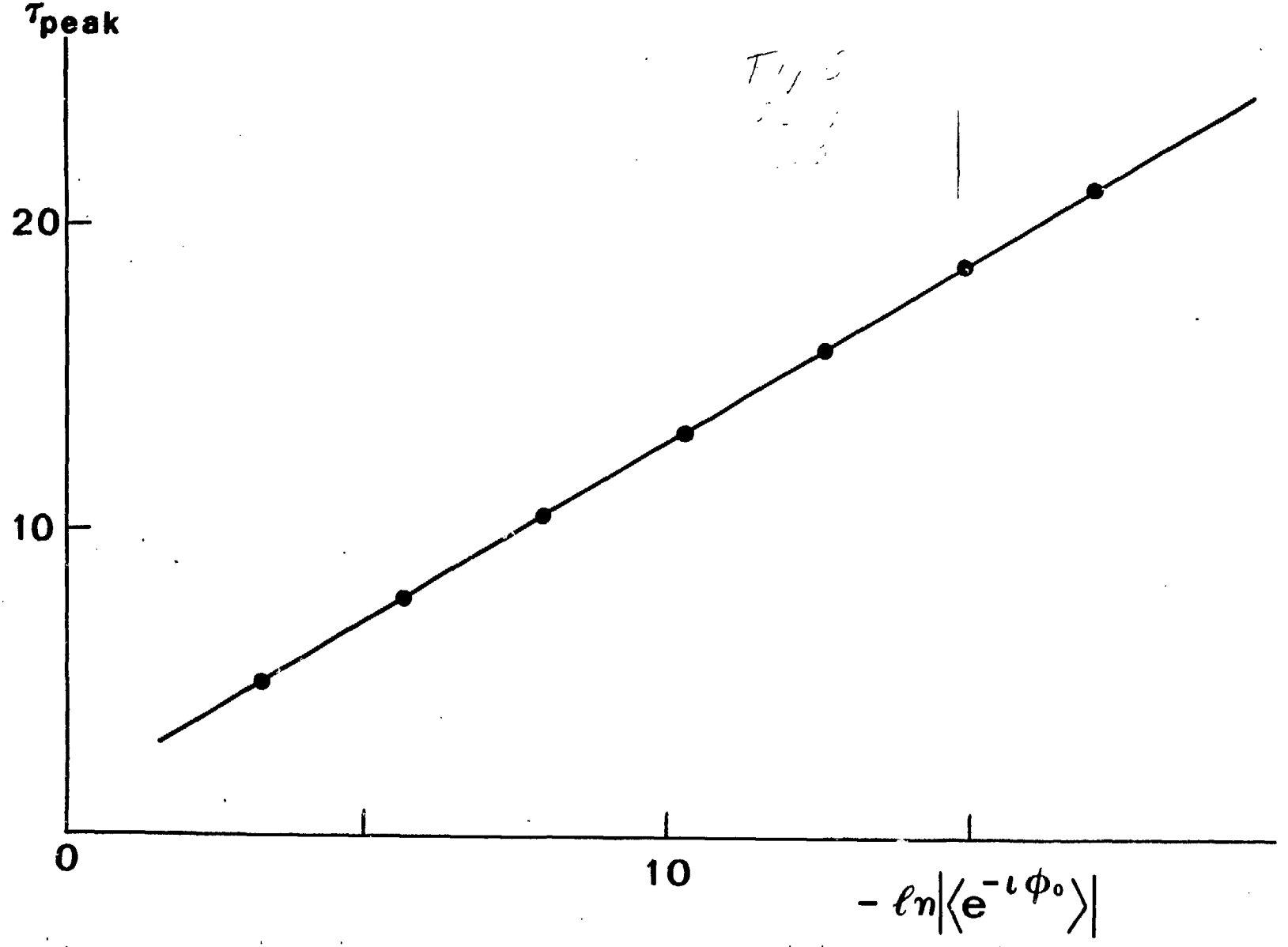
τ_{peak}
20
10
0
10
$-\ell n\left|\left\langle e^{-i\phi_0}\right\rangle\right|$

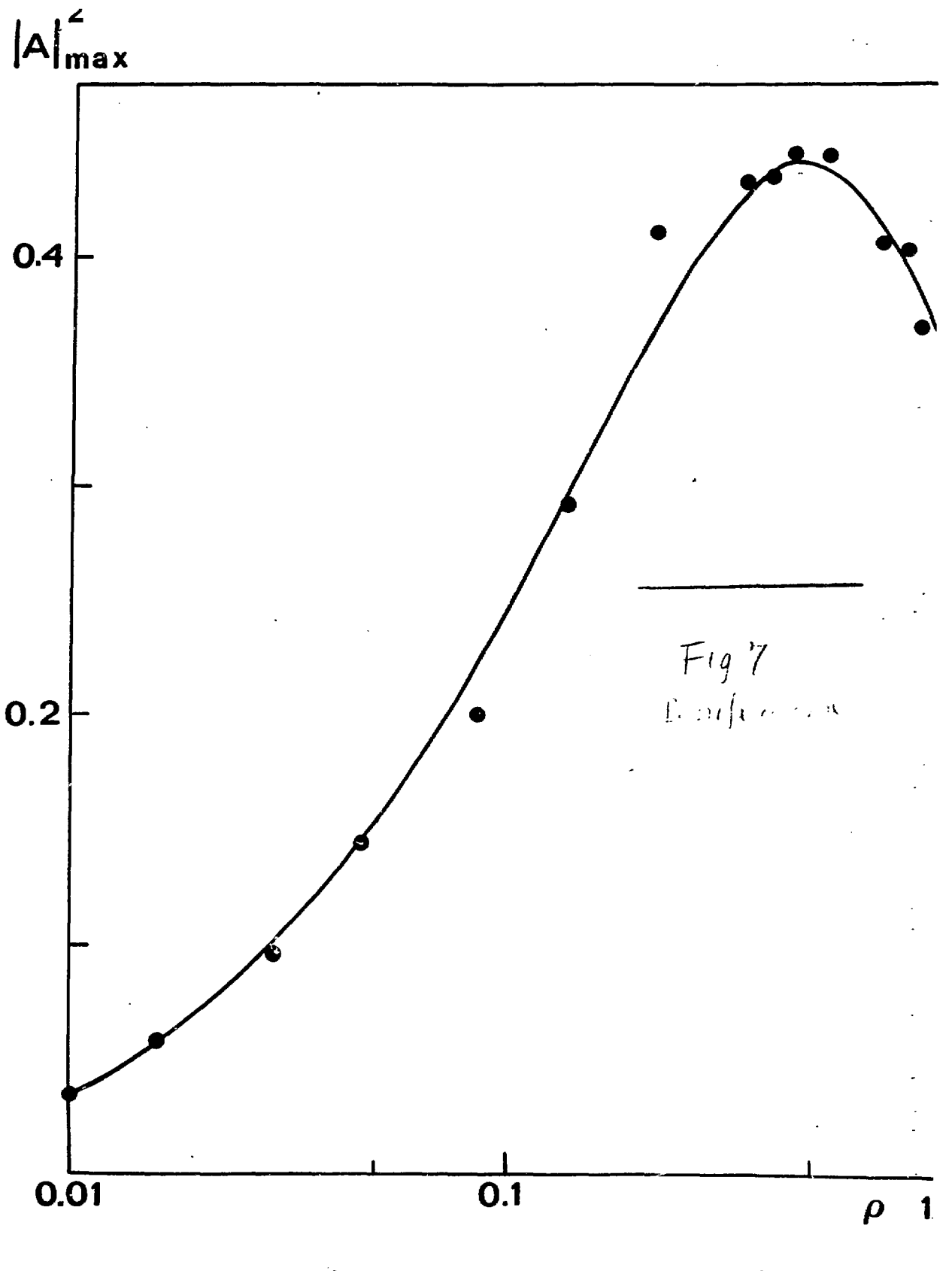

Fig 7

Fig. 8

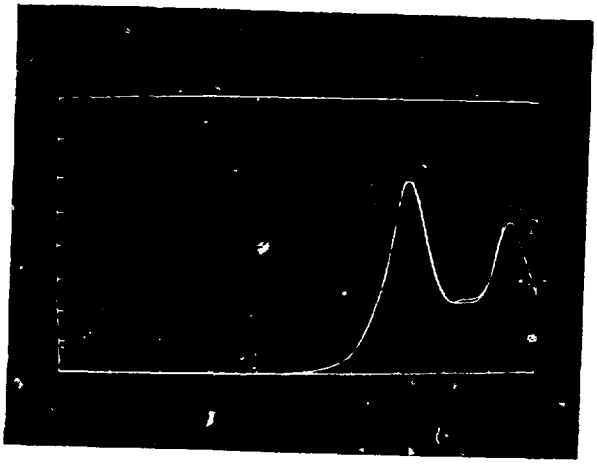

Fig 9